Research Article Vol. 5, No. 10 / October 2018 / Optica 1283

Propagation-enhanced generation of intense high-harmonic continua in the 100-eV spectral region

D. E. Rivas,[1,2,11,12,†] B. Major,[3,4,†] M. Weidman,[1] W. Helml,[2,5] G. Marcus,[1,6] R. Kienberger,[1,5] D. Charalambidis,[4,7,8] P. Tzallas,[4,7] E. Balogh,[3] K. Kovács,[9] V. Tosa,[9] B. Bergues,[1,2] K. Varjú,[3,4] and L. Veisz[1,10,*]

[1]Max-Planck-Institut für Quantenoptik, Hans-Kopfermann Strasse 1, 85748 Garching, Germany
[2]Fakultät für Physik, Ludwig-Maximilians-Universität München, Am Coulombwall 1, 85748 Garching, Germany
[3]Department of Optics and Quantum Electronics, University of Szeged, Dóm tér 9, Szeged 6720, Hungary
[4]ELI-ALPS, ELI-HU Non-Profit Ltd., Dugonics ter 13, Szeged 6720, Hungary
[5]Physics Department, Technische Universität München, James-Frank-Str. 1, 85748 Garching, Germany
[6]Department of Applied Physics, The Hebrew University of Jerusalem, Jerusalem 91904, Israel
[7]FORTH-IESL, PO Box 1527, GR-711 10 Heraklion, Crete, Greece
[8]Department of Physics, University of Crete, PO Box 2208, GR71003 Heraklion, Crete, Greece
[9]National Institute for R&D of Isotopic and Molecular Technologies, Donath 67-103, 400293 Cluj-Napoca, Romania
[10]Department of Physics, Umeå University, SE-901 87 Umeå, Sweden
[11]Current address: European XFEL GmbH, Holzkoppel 4, 22869 Schenefeld, Germany
[12]e-mail: daniel.rivas@xfel.eu
*Corresponding author: laszlo.veisz@umu.se

Received 10 July 2018; revised 17 September 2018; accepted 17 September 2018 (Doc. ID 338395); published 12 October 2018

The study of core electron dynamics through nonlinear spectroscopy requires intense isolated attosecond extreme ultraviolet or even X-ray pulses. A robust way to produce these pulses is high-harmonic generation (HHG) in a gas medium. However, the energy upscaling of the process depends on a very demanding next-generation laser technology that provides multi-terawatt (TW) laser pulses with few-optical-cycle duration and controlled electric field. Here, we revisit the HHG process driven by 16-TW sub-two-cycle laser pulses to reach high intensity in the 100-eV spectral region and beyond. We show that the combination of above barrier-suppression intensity with a long generation medium significantly enhances the isolation of attosecond pulses compared to lower intensities and/or shorter media and this way reduces the pulse duration as well as field-stability requirements on the laser driver. This novel regime facilitates the real-time observation of electron dynamics at the attosecond timescale in atoms, molecules, and solids.

https://doi.org/10.1364/OPTICA.5.001283

1. INTRODUCTION

In the past years, tabletop sources of extreme ultraviolet radiation have reached the long-sought capability for nonlinear spectroscopy in atoms [1–7] and molecules [8–10]. These sources are based on the conversion of intense near-infrared (NIR) laser pulses to high-order harmonics of their central frequency [11,12]. Due to the highly nonlinear nature of the conversion process, they offer a temporal resolution well below an optical cycle of the driving laser. This permits the study of electron dynamics in their natural few-femtosecond to attoseconds timescales [13], extending on the current state of the art established at free-electron laser (FEL) facilities [14].

In the high-harmonic generation (HHG) process, the conversion efficiency between the driving laser and the harmonic radiation is generally low [15], and it further decreases when generating higher photon energies [16]. Therefore, to reach the necessary extreme ultraviolet (XUV) to x-ray intensities for sub-femtosecond (fs) nonlinear spectroscopy, these sources ultimately require high-energy driving lasers. In such systems, meeting the requirements for the generation of isolated attosecond pulses is very demanding. The combination of the necessary high pulse energies together with few-cycle pulse durations, accurate carrier-envelope phase (CEP) control, and few-percent intensity stability is still not readily available and is a topic of active development [17–19].

Previous research with high-energy multi-cycle driving pulses has shown that combining high driving intensities together with long generation media leads to an initial self-modulation followed by a steady propagation of the driving pulse [20–25]. During the HHG process XUV pulse trains are produced and the NIR laser pulses propagate for several centimeters without significantly changing their properties, resulting in relaxed

requirements on input energy stability in addition to employing more compact setups.

On the other hand, HHG in short highly ionized media implies relaxed requirements on the pulse duration for the isolation of attosecond pulses, a process known as ionization gating or transient phase-matching gating [26–33]. In this regime, usually achieved with lower-energy few-cycle pulses, the rapid change in electron density leads to a reduced phase-matching time window. As a consequence, the bandwidth over which an attosecond pulse can be isolated is extended.

In this work, we show that for high-energy few-cycle pulses, the combination of steady propagation together with transient phase matching leads to the robust generation of high-harmonic quasi-continua at 100 eV. Through single-shot XUV characterization, we show that for long medium lengths, the spatiospectral properties of the emitted XUV radiation exhibit low CEP dependence and feature a broader continuum region and thus strongly differ from what is obtained from shorter media or at lower intensities. We reproduce the spatially resolved spectral measurements with a three-dimensional nonadiabatic model that provides experimentally unrevealed details about the process. The calculations confirm that under these conditions efficient harmonic emission at the cutoff region is limited to an isolated event in time.

2. HHG IN A LONG GAS CELL

The experimental setup for the generation of the intense pulses in the 100-eV spectral region and its application for the study of nonlinear dynamics from inner-atomic shells of xenon are described elsewhere [7]. As a summary, the HHG process is driven by the Light Wave Synthesizer 20, providing NIR pulses with an on-target energy of up to 40 mJ, pulse durations down to 4.3 fs, and unstabilized CEP [19]. By employing a 17-m focal length spherical mirror, the pulses are focused into different neon gas targets, to an intensity of approximately 2×10^{15} W/cm^2. This value exceeds the barrier-suppression intensity (BSI) for neon ($\sim 8.6 \times 10^{14}$ W/cm^2), which indicates that the generation medium is highly ionized, a condition necessary to achieve transient phase matching.

Despite the above-threshold intensity level in our experiment, a conversion efficiency from NIR to XUV of 10^{-6} is achieved by generating up to 40 nJ of energy in a spectral range from approximately 60 eV (due to the transmission of the Zr filters employed for filtering out the driving NIR beam) to a cutoff energy of 130 eV. This energy value is obtained considering only the on-axis radiation reaching our detectors, thus neglecting any possible additional off-axis contribution (see Discussion). To achieve the optimum efficiencies, we focused the driving laser at the entrance of a 10-cm gas cell filled with neon at a backing pressure of 20–30 mbar, which corresponds to an estimated 5–10 mbar inside the cell. The measured efficiency in this spectral region is in accordance with values reported with less energetic sub-5-fs laser drivers in this spectral region [30,34].

The high energy content of the XUV pulses allows the single-shot measurement of both pulse energy and spatially resolved spectra [see Figs. 1(a) and 1(b)]. This is done with an energy photodiode and a homemade XUV spectrometer, respectively [7]. The acquired spectra exhibit distinct features that remain constant from shot to shot, despite the random CEP of the driver laser (see Supplement 1 for additional single-shot images). In particular, the expected changes between modulated and continuous spectra in the cutoff region [35] are not observed, but rather a relatively stable and broad quasi-continuum, supporting the interpretation

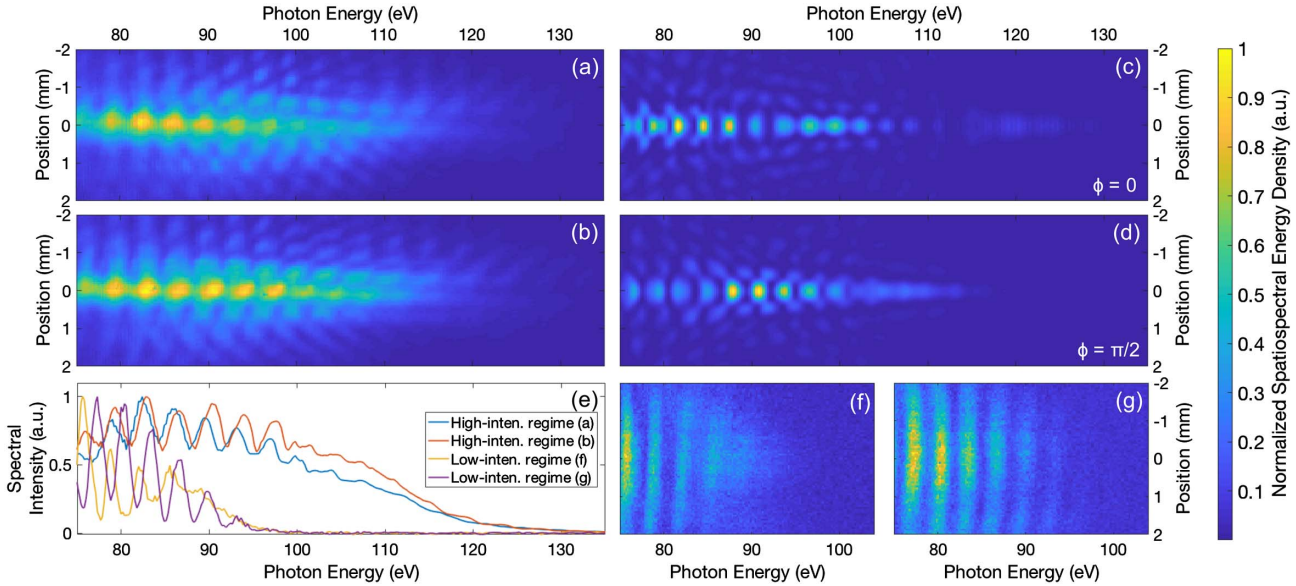

Fig. 1. (a) and (b) Two single-shot measurements of the spatiospectral energy density distribution of the XUV beam generated from the 10 cm neon gas cell at optimum conditions (NIR laser intensity of $\sim 2 \times 10^{15}$ W/cm^2). The measurement reveals slight spectral modulations, a cutoff energy at approximately 130 eV (2% shot-to-shot RMS stability), and the presence of off-axis even harmonics. Spatiospectral energy density distribution from our theoretical model for a CEP of (c) $\phi_{\mathrm{CEP}} = 0$, and (d) $\phi_{\mathrm{CEP}} = \pi/2$. The calculation accurately reproduces the features observed in the single-shot measurements. (e) Comparison of the on-axis lineout of the measured spatiospectral energy density at high and low intensities. (f) and (g) Two single-shot measurements of the spatiospectral energy density distribution of the XUV beam generated from the 10 cm neon gas cell at a reduced intensity of 5×10^{14} W/cm^2. At this intensity the expected changes between modulations and continuum in the cutoff-energy region are recovered.

of isolating intense XUV pulses of sub-optical-cycle duration (see Discussion below).

To exclude that this effect is due to a lack of resolution of our spectrometer, we close an aperture before the focusing mirror, reducing the intensity to below 5×10^{14} W/cm^2. This causes a significant reduction in the XUV pulse energy, but the single-shot spectral characterization is still possible. Under this below-threshold intensity condition, the expected spectral behavior is recovered: strong modulations are observed in the plateau region, and the cutoff-region modulation varies from shot to shot [19] [see Figs. 1(e)–1(g) and additional shots in Supplement 1]. Furthermore, the broadest continuum region is around 10 eV in bandwidth, which is two to three times narrower than at higher intensities. This confirms that at high intensities our results are in agreement with the expected behavior from the transient phase-matching regime [26,30].

For a better understanding of the dynamics underlying the generation process, a three-dimensional nonadiabatic simulation model is used to reproduce the experimental results [23,36,37]. We first calculate the spatiotemporal distribution of the driving electric field at the entrance of the interaction region matched to the measured intensity profile at the target plane (for additional details, see Supplement 1 on intensity measurement and calculation). A peak intensity of 1.6×10^{15} W/cm^2, a beam size of 360 μm full width at half-maximum (FWHM), and a pulse duration of 4.5 fs are used as input conditions.

The calculated driving electric field is then used as the input for the theoretical model, which calculates the HHG process in three steps (additional details on the model are provided in Supplement 1). First, the propagation of the driving laser field is calculated, assuming a cylindrical symmetry based on the nonlinear wave equation over the 10 cm length of neon gas at a pressure of 7 mbar. Having the temporal evolution of the electric field in the whole simulated volume, the single-atom response of the medium is then determined. Finally, the wave equation is solved for the harmonic field using the time-dependent macroscopic dipole as the source term (the resulting single-atom response and harmonic distribution are included in Supplement 1). For comparison with the measured spatiospectral energy distribution, the calculated harmonic field is propagated over a distance of 12 m and then filtered by the theoretical transmission of 300 nm of Zr, as in the experimental setup.

The calculated spatiospectral energy density distributions [see Figs. 1(c) and 1(d)] are in good agreement with the measured single-shot spectra. Besides the matching cutoff energy of 130 eV and beam divergence of approximately 0.1 mrad, additional features are reproduced, such as the presence of off-axis even harmonics, which are a consequence of the sub-cycle changes in the phase-matching conditions.

3. HHG IN SHORTER MEDIA

To understand the effects of propagation, we reduce the medium length with respect to the optimum length of 10 cm. As an extreme case, we first use a supersonic gas jet of 1.5 mm output diameter [38]. This jet ensures a short propagation through the gas by providing a flat-top gas density distribution profile. An optimum efficiency is obtained when focusing the laser directly at the jet, with a backing pressure of 3–5 bar, which corresponds to a gas pressure of a few hundred millibar (mbar) in the interaction region. The overall XUV-pulse energy under phase-matching conditions reaches approximately 4 nJ in the Zr transmission window, i.e., an order of magnitude less than with the 10 cm cell.

When the laser pulses have a short propagation length, the emitted harmonic radiation is expected to have a stronger dependence on the input laser conditions. This is reflected by the observation of strong shot-to-shot changes in the measured spatiospectral energy density distribution. Despite the observation of a higher cutoff energy and the recovery of stronger spectral modulations, the radial distribution of the emitted radiation randomly varies between an on-axis [see Fig. 2(a)] and off-axis [see Fig. 2(b)] distribution (see additional shots in Supplement 1). Unlike previous observations of ring-like harmonic beam profiles [39], the effect is observed both for the medium being before and after the focus.

In the cutoff region, an off-axis continuum is observed [as in Fig. 2(b)], but modulations are always present on-axis. As a consequence, the extraction of an isolated attosecond pulse would not be possible without post-selecting the continuum region through spatial filtering. To the best of our knowledge, the strong dependence of the spatiospectral energy density distribution as a function of CEP has not been reported before. We attribute this to the fact that with standard millijoule scale lasers, a high-pressure medium length shorter than 100 μm is needed to observe this effect, which can be technically challenging.

We use the theoretical model again to calculate the harmonic emission, with the same laser parameters as for the 10 cm cell, but now for a 1.5 mm long neon medium at 240 mbar. Again, the measured spectra are well reproduced by our calculations, agreeing in the generated photon energies as well as the observed changes in spatiospectral energy-density distribution [see Figs. 2(d) and 2(e)]. To understand the source of the measured changes in energy-density distribution, we performed the same calculation but with a variation of the experimental parameters, such as CEP, driving laser intensity, and target gas pressure. These series of calculations revealed that such big fluctuations can only be attributed to the randomly varying CEP, within the measured stability of our experimental parameters.

We investigated the transition between these two different regimes by additionally employing a cell with an intermediate length of 5 cm, under similar driving-laser conditions. In this case, the spatiospectral properties of the emitted radiation are again stable from shot to shot in comparison to the shorter medium. However, the distribution of the energy-density differs from the 10 cm long cell, despite reaching comparable conversion efficiencies. The off-axis radiation is still present when compared to the results with the 10 cm cell. The off-axis radiation reaches a slightly higher cutoff energy than with the 10 cm cell, but is lower than what is observed with the gas jet, in addition to strong modulations over the whole transversal region [see Fig. 2(c)]. Thus, the isolation of an attosecond pulse is not possible after only 5 cm propagation. Again, as in the previous cases, the theoretical model correctly reproduces our experimental observations [see Fig. 2(f)].

A comparison between the three different regimes leads to the conclusion that long propagation media are necessary for having an efficient and stable high-harmonic beam with a quasi-continuous spectrum independently from the laser CEP. Additionally, the good agreement between our experiments and the theoretical model validates its use for the understanding of the underlying dynamics of the generation process.

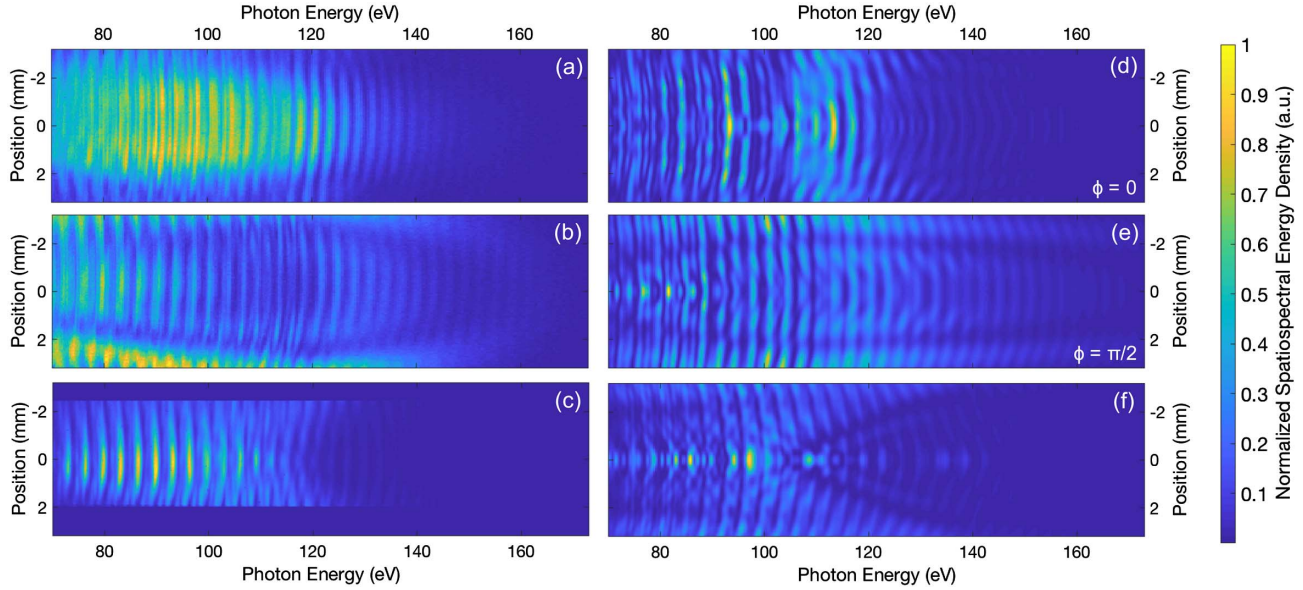

Fig. 2. Single-shot measurement of the spatiospectral energy density distribution of the XUV beam generated from the 1.5 mm neon gas jet, exhibiting (a) on-axis and (b) off-axis emission. In the experiment, the spatial energy-density distribution varies randomly from shot to shot (see additional shots in Supplement 1). (c) Single-shot measurement of the spatiospectral energy density distribution of the XUV beam generated from the 5 cm gas cell. Significant energy is present off-axis in comparison to Fig. 1, (a)–(b), showing also a higher cutoff energy. Additionally, spectral modulations are visible throughout the whole measured region, not allowing the isolation of single pulses. The lack of signal at radii above 2 mm is due to changes in the detector's clear aperture, unrelated to these specific measurements. Calculated spatially resolved spectra for a 1.5 mm length gas jet for a CEP value of (d) $\phi_{\mathrm{CEP}} = 0$ and (e) $\phi_{\mathrm{CEP}} = \pi/2$. Only the changes obtained when varying the CEP can accurately reproduce the differences between (a) and (b). (f) Calculated spatially resolved spectra for the 5 cm cell, again reproducing the features of the spectrum shown in (c).

4. DISCUSSION

We first investigate the driving laser propagation through the gas medium. From the calculated spatial distribution of the temporal peak intensity, two separate regions along the propagation length can be identified [see Figs. 3(a) and 3(b)]. During the first 3–4 cm of propagation, a strong reshaping occurs, where the on-axis intensity quickly decreases, leading to a quasi-flat-top beam profile. Then, for the remaining part of the gas cell, the beam propagates in a steady regime with a relatively constant peak intensity of approximately 8×10^{14} W/cm^2. This intensity is slightly below the BSI for neon.

Upon variations of the input intensity in the order of 10% [higher than our measured root mean square (RMS) peak fluence fluctuations of 4%] the self-stabilization still leads to approximately the same on-axis intensity [see Fig. 3(b)]. This reshaping and propagation effects results in an attractor with optimal conditions for robust generation of harmonics, relatively independent of input laser conditions.

The radially dependent input peak intensity leads to significant differences in the ionization fraction in the radial coordinate (40% at $r = 0$, while only 0.6% at $r = 250$ μm, while the intensity FWHM beam waist is 360 μm). Upon propagation, this causes an ionization defocusing, which increases in time for the duration of the laser pulse. This is equivalent to a stronger ionization-induced blueshift in the central region in comparison to >0 radii, or in other words, to a self-induced dynamic wavefront bending, also called the ionization-induced light-house effect [40,41] as shown in Fig. 3(c). At the output of the cell, the on-axis ionization reaches a value of 2.9%, which is in agreement with previous results on transient phase matching [29]. However, our model additionally allows the further investigation of the off-axis behavior and how this wavefront affects the spatial isolation of the generated attosecond pulses.

To this end, we now analyze the spatiotemporal intensity distribution of the emitted XUV pulses at the detector plane located 12 m from the output of the cell. To understand the effects of propagation, we compare the results calculated for the 1.5 mm gas jet, the 5 cm cell, and 10 cm cell. Before calculating the intensity distribution, we spectrally filter the harmonic spectra in accordance with the theoretical transmission of the 300 nm Zr filter and the calculated reflectivity curve of the XUV mirror used in previous two-photon absorption experiments [7,42,43]. The multilayer XUV mirror provides a 11 eV (FWHM) band-pass filter at a photon energy of 115 eV, corresponding to the continuum spectral region.

For an input CEP of $\phi_{\mathrm{CEP}} = 0$ (defined at the plane of the focusing optic and thus shifting by approximately $\pi/2$ when focusing), the radiation coming from the 1.5 mm jet and 5 cm cell is distributed over a wide area, and double pulses are obtained on axis [see Figs. 4(a) and 4(b)]. However, if the driving laser propagates for 10 cm in the generation medium, the two sequential attosecond pulses become spatiotemporally separated at the detector plane [see Fig. 4(c)].

With the goal of achieving high intensities for nonlinear XUV spectroscopy, we calculate the spatially resolved instantaneous intensity after focusing [see Fig. 4(d)]. The focal length of the mirror is chosen to be 12.5 mm, like the one used in the previous two-photon absorption experiments [7]. The pulses generated from different half cycles (region 1 and 2, enclosed with a green and red circle, respectively) do not focus at the same plane. This arises due to their different divergence, a consequence of the dynamic wavefront bending experienced by the driving laser

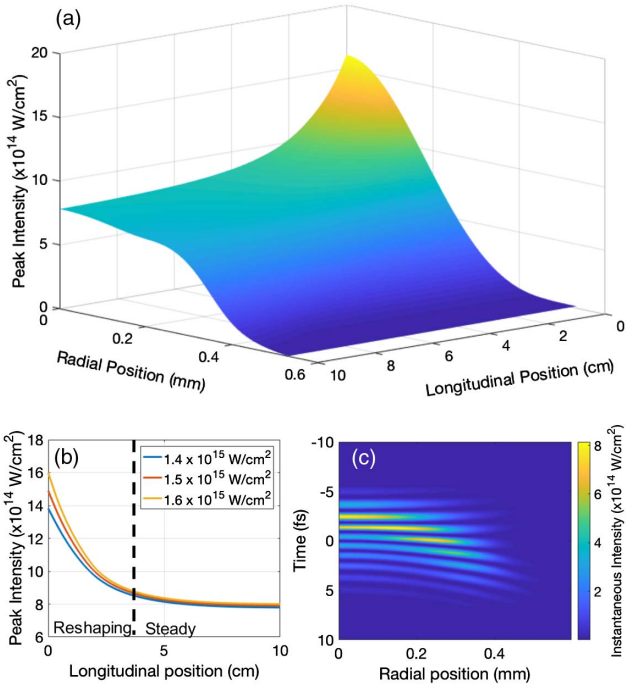

Fig. 3. (a) Spatial distribution of the driving laser peak intensity inside the 10 cm gas cell. Two different regions can be distinguished: the reshaping and the steady regions [separated by dashed line in (b)]. After a strong intensity decrease in the reshaping region, the beam acquires a flat-top shape with a stable intensity value around 8×10^{14} W/cm^2. (b) On-axis intensity as a function of cell length, for an intensity of 1.4×10^{15}, 1.5×10^{15}, and 1.6×10^{15} W/cm^2. The same stabilized peak intensity value is achieved after propagation for the three values of the input intensity. (c) Spatially resolved instantaneous intensity at the cell's output plane. Due to the large differences in ionization as a function of radius, a dynamic wavefront bending is induced upon propagation.

in the ionized medium. Experimentally, this allows the spatial isolation of the attosecond pulses before focusing, i.e., through an aperture, or in the near field, through a detector with spatial resolution [44].

Finally, we seek to understand the dependence of the spatially resolved intensity distribution with varying CEP. In the experiment, relative low shot-to-shot fluctuations are observed irrespective of the randomly varying CEP. For the 10 cm long gas cell, we compare the spatially resolved intensity at the detector plane for an input CEP of $\phi_{\mathrm{CEP}} = 0$, $\phi_{\mathrm{CEP}} = \pi/4$, and $\phi_{\mathrm{CEP}} = \pi/2$ [see Figs. 5(a)–5(c)]. For all three CEP values, the spatiotemporal isolation still holds, only with changes in relative amplitude and spatial distribution. The on-axis lineouts over a radius of 1 mm show a contrast ratio better than 1:10 between the main and the secondary pulses, which is not achieved with the 5 cm cell [see Figs. 5(d)–5(f)]. This result extends the transient phase-matching regime by the additional spatiotemporal isolation, independent of the input laser waveform.

In conclusion, we demonstrate that for the energy scaling of HHG-based XUV attosecond pulses towards time-resolved nonlinear spectroscopy, the combination of intensities above the BSI with long propagation in the generation medium is advantageous. In comparison to lower intensities or shorter media, the reshaping experienced by the driving laser mitigates the fluctuations of the input conditions while at the same time leads to a spatiotemporal isolation of the XUV pulses independently from the original laser CEP. With the current advances in femtosecond laser technology, our demonstration establishes a robust path for the development of future intense XUV and x-ray sources. The good agreement between the measurements and the theoretical model allows the further tailoring and optimization of these sources, supporting the current world-wide efforts towards the development laboratory-scale nonlinear attosecond spectroscopy [2,45–47].

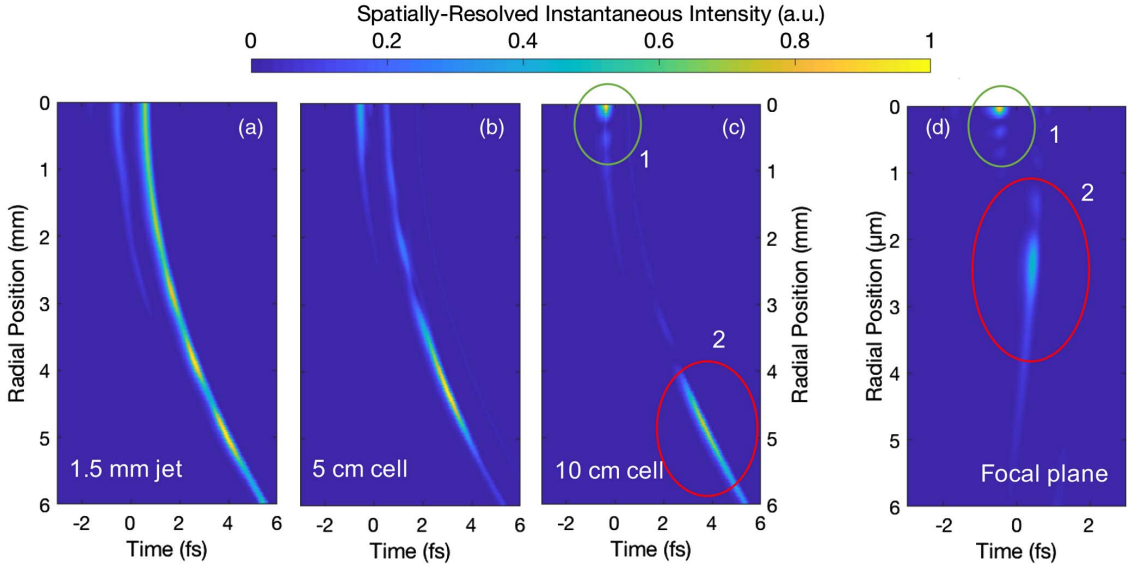

Fig. 4. Normalized spatially resolved instantaneous intensity of harmonics at the cutoff-energy region (115 eV, 11 eV bandwidth), arising from the (a) 1.5 mm jet, (b) 5 cm cell, and (c) 10 cm cell, at the detector plane located 12 m away from the generation target. For the first two cases, the radiation is distributed over a wide area, and double pulses are obtained on axis. However, with the 10 cm long cell, the on- and off-axis radiation (region 1, green circle and region 2, red circle, respectively) becomes spatiotemporaly isolated in the detector plane. (d) After focusing the pulses with a 12.5 mm mirror, the spatial separation of the two sequential pulses is maintained due to their different divergence, caused by dynamic wavefront bend of the driving laser.

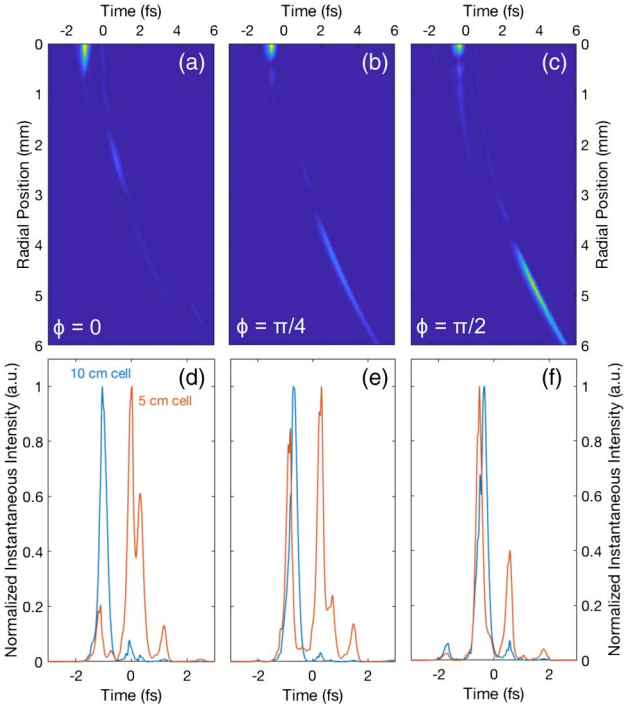

Fig. 5. Normalized spatially resolved instantaneous intensity of harmonics at the cutoff-energy region (115 eV, 11 eV bandwidth), for the 10 cm long gas cell, for an input CEP of (a) $\phi_{CEP} = 0$, (b) $\phi_{CEP} = \pi/4$, and (c) $\phi_{CEP} = \pi/2$ at the detector plane 12 m away from the cell's output [same plot as Fig. 4(c)]. For all three CEP values, the spatiotemporal isolation is maintained. Comparison of the on-axis ($r < 1$ mm) normalized instantaneous intensity between the 5 cm (red line) and 10 cm cell (blue line) for an input CEP of (d) $\phi_{CEP} = 0$, (e) $\phi_{CEP} = \pi/4$, and (f) $\phi_{CEP} = \pi/2$, at the detector plane. In comparison, the on-axis temporal isolation is not yet achieved after only 5 cm propagation for all three CEP values.

Funding. Munich-Centre for Advanced Photonics (MAP); Laserlab-Europe (MPQ002119); H2020 Euratom (EURATOM) (633053); H2020 European Research Council (ERC); European Regional Development Fund (ERDF) (GINOP-2.3.6-15-2015-00001); Vetenskapsrådet (VR) (2016-05409); Competitiveness, Entrepreneurship and Innovation (NSRF 2014-2020); ANCSI 03ELI/2016 (PROPW); HELLAS-CH (MIS 5002735).

Acknowledgment. We are grateful for fruitful discussions with Hartmut Schröder, Eleftherios Goulielmakis, Alexander Guggenmos, and Ferenc Krausz, and we further acknowledge the technical support offered by Harald Haas, Anton Horn, Tobias Kleinhenz, Walter Ritt, and Manfred Fischer. We acknowledge KIF for giving us access to supercomputing resources based in Hungary at Debrecen and at Szeged. We are also grateful for the access to the Data Center at INCDTIM Cluj-Napoca. HELLAS-CH is co-financed by Greece and the European Union-European Regional Development Fund

†These authors contributed equally for this work.

See Supplement 1 for supporting content.

REFERENCES

1. T. Sekikawa, A. Kosuge, T. Kanai, and S. Watanabe, "Nonlinear optics in the extreme ultraviolet," Nature **432**, 605–608 (2004).
2. K. Midorikawa, Y. Nabekawa, and A. Suda, "XUV multiphoton processes with intense high-order harmonics," Prog. Quantum Electron. **32**, 43–88 (2008).
3. P. Tzallas, E. Skantzakis, L. A. A. Nikolopoulos, G. D. Tsakiris, and D. Charalambidis, "Extreme-ultraviolet pump-probe studies of one femtosecond scale electron dynamics," Nat. Phys. **7**, 781–784 (2011).
4. B. Manschwetus, L. Rading, F. Campi, S. Maclot, H. Coudert-Alteirac, J. Lahl, H. Wikmark, P. Rudawski, C. M. Heyl, B. Farkas, T. Mohamed, A. L'Huillier, and P. Johnsson, "Two-photon double ionization of neon using an intense attosecond pulse train," Phys. Rev. A **93**, 061402 (2016).
5. N. Tsatrafyllis, B. Bergues, H. Schröder, L. Veisz, E. Skantzakis, D. Gray, B. Bodi, S. Kuhn, G. D. Tsakiris, D. Charalambidis, and P. Tzallas, "The ion microscope as a tool for quantitative measurements in the extreme ultraviolet," Sci. Rep. **6**, 21556 (2016).
6. T. R. Barillot, P. Matia-Hernando, D. Greening, D. J. Walke, T. Witting, L. J. Frasinkski, J. P. Marangos, and J. W. G. Tisch, "Towards XUV pump-probe experiments in the femtosecond to sub-femtosecond regime: new measurement of the helium two-photon ionization cross-section," Chem. Phys. Lett. **683**, 38–42 (2017).
7. B. Bergues, D. E. Rivas, M. Weidman, A. A. Muschet, W. Helml, A. Guggenmos, V. Pervak, U. Kleineberg, G. Marcus, R. Kienberger, D. Charalambidis, P. Tzallas, H. Schröder, F. Krausz, and L. Veisz, "Tabletop nonlinear optics in the 100-eV spectral region," Optica **5**, 237–242 (2018).
8. P. A. Carpeggiani, P. Tzallas, A. Palacios, D. Gray, F. Martín, and D. Charalambidis, "Disclosing intrinsic molecular dynamics on the 1-fs scale through extreme-ultraviolet pump-probe measurements," Phys. Rev. A **89**, 023420 (2014).
9. T. Okino, Y. Furukawa, Y. Nabekawa, S. Miyabe, A. A. Eilanlou, E. J. Takahashi, K. Yamanouchi, and K. Midorikawa, "Direct observation of an attosecond electron wave packet in a nitrogen molecule," Sci. Adv. **1**, e1500356 (2015).
10. Y. Nabekawa, Y. Furukawa, T. Okino, A. A. Eilanlou, E. J. Takahashi, K. Yamanouchi, and K. Midorikawa, "Sub-10-fs control of dissociation pathways in the hydrogen molecular ion with a few-pulse attosecond pulse train," Nat. Commun. **7**, 12835 (2016).
11. A. McPherson, G. Gibson, H. Jara, U. Johann, T. S. Luk, I. A. McIntyre, K. Boyer, and C. K. Rhodes, "Studies of multiphoton production of vacuum-ultraviolet radiation in the rare gases," J. Opt. Soc. Am. B **4**, 595–601 (1987).
12. M. Ferray, A. L'Huillier, X. F. Li, L. A. Lompre, G. Mainfray, and C. Manus, "Multiple-harmonic conversion of 1064 nm radiation in rare gases," J. Phys. B **21**, L31–L35 (1988).
13. F. Krausz and M. Ivanov, "Attosecond physics," Rev. Mod. Phys. **81**, 163–234 (2009).
14. W. Helml, I. Grguraš, P. N. Juranić, S. Düsterer, T. Mazza, A. R. Maier, N. Hartmann, M. Ilchen, G. Hartmann, L. Patthey, C. Callegari, J. T. Costello, M. Meyer, R. N. Coffee, A. L. Cavalieri, and R. Kienberger, "Ultrashort free-electron laser x-ray pulses," Appl. Sci. **7**, 915 (2017).
15. P. Rudawski, C. M. Heyl, F. Brizuela, J. Schwenke, A. Persson, E. Mansten, R. Rakowski, L. Rading, F. Campi, B. Kim, P. Johnsson, and A. L'Huillier, "A high-flux high-order harmonic source," Rev. Sci. Instrum. **84**, 073103 (2013).
16. T. Popmintchev, M.-C. Chen, A. Bahabad, M. Gerrity, P. Sidorenko, O. Cohen, I. P. Christov, M. M. Murnane, and H. C. Kapteyn, "Phase matching of high harmonic generation in the soft and hard X-ray regions of the spectrum," Proc. Natl. Acad. Sci. USA **106**, 10516–10521 (2009).
17. E. Cunningham, Y. Wu, and Z. Chang, "Carrier-envelope phase control of a 10 Hz, 25 TW laser for high-flux extreme ultraviolet quasi-continuum generation," Appl. Phys. Lett. **107**, 201108 (2015).
18. R. Budriunas, T. Stanislauskas, J. Adamonis, A. Aleknavičius, G. Veitas, D. Gadonas, S. Balickas, A. Michailovas, and A. Varanavičius, "53 W average power CEP-stabilized OPCPA system delivering 5.5 TW few cycle pulses at 1 kHz repetition rate," Opt. Express **25**, 5797–5806 (2017).
19. D. E. Rivas, A. Borot, D. E. Cardenas, G. Marcus, X. Gu, D. Herrmann, J. Xu, J. Tan, D. Kormin, G. Ma, W. Dallari, G. D. Tsakiris, I. B. Földes, S.-W. Chou, M. Weidman, B. Bergues, T. Wittmann, H. Schröder, P. Tzallas, D. Charalambidis, O. Razskazovskaya, V. Pervak, F. Krausz, and L. Veisz, "Next generation driver for attosecond and laser-plasma physics," Sci. Rep. **7**, 5224 (2017).
20. Y. Tamaki, J. Itatani, Y. Nagata, M. Obara, and K. Midorikawa, "Highly efficient, phase-matched high-harmonic generation by a self-guided laser beam," Phys. Rev. Lett. **82**, 1422–1425 (1999).

21. M. Bellini, C. Corsi, and M. C. Gambino, "Neutral depletion and beam defocusing in harmonic generation from strongly ionized media," Phys. Rev. A **64**, 023411 (2001).
22. V. Tosa, E. Takahashi, Y. Nabekawa, and K. Midorikawa, "Generation of high-order harmonics in a self-guided beam," Phys. Rev. A **67**, 063817 (2003).
23. V. Tosa, K. T. Kim, and C. H. Nam, "Macroscopic generation of attosecond-pulse trains in strongly ionized media," Phys. Rev. A **80**, 045801 (2009).
24. C. Vozzi, M. Negro, F. Calegari, S. Stagira, K. Kovács, and V. Tosa, "Phase-matching effects in the generation of high-energy photon by mid-infrared few-cycle laser pulses," New J. Phys. **13**, 073003 (2011).
25. B. Schütte, P. Weber, K. Kovács, E. Balogh, B. Major, V. Tosa, S. Han, M. J. J. Vrakking, K. Varju, and A. Rouzée, "Bright attosecond soft X-ray pulse trains by transient phase-matching in two-color high-order harmonic generation," Opt. Express **23**, 33947–33955 (2015).
26. T. Pfeiffer, A. Jullien, M. J. Abel, P. M. Nagel, L. Gallmann, D. M. Neumark, and S. R. Leone, "Generating coherent broadband continuum soft-x-ray radiation by attosecond ionization gating," Opt. Express **15**, 17120–17128 (2007).
27. V. V. Strelkov, E. Mével, and E. Constant, "Generation of isolated attosecond pulses by spatial shaping of a femtosecond laser beam," New J. Phys. **10**, 083040 (2008).
28. I. Thomann, A. Bahabad, X. Liu, R. Trebino, M. M. Murnane, and H. C. Kapteyn, "Characterizing isolated attosecond pulses from hollow-core waveguides using multi-cycle driving pulses," Opt. Express **17**, 4611–4633 (2009).
29. M. J. Abel, T. Pfeifer, P. M. Nagel, W. Boutu, M. J. Bell, C. P. Steiner, D. M. Neumark, and S. R. Leone, "Isolated attosecond pulses from ionization gating of high-harmonic emission," Chem. Phys. **366**, 9–14 (2009).
30. F. Ferrari, F. Calegari, M. Lucchini, C. Vozzi, S. Stagira, G. Sansone, and M. Nisoli, "High-energy isolated attosecond pulses generated by above-saturation few-cycle fields," Nat. Photonics **4**, 875–879 (2010).
31. M.-C. Chen, C. Mancuso, C. Hernández-García, F. Dollar, B. Galloway, D. Popmintchev, P.-C. Huang, B. Walker, L. Plaja, A. A. Jaroń-Becker, A. Becker, M. M. Murnane, H. C. Kapteyn, and T. Popmintchev, "Generation of bright isolated attosecond soft x-ray pulses driven by multicycle midinfrared lasers," Proc. Natl. Acad. Sci. USA **111**, E2361–E2367 (2014).
32. C. Hernandez-Garcia, T. Popmintchev, M. M. Murnane, H. C. Kapteyn, L. Plaja, A. Becker, and A. Jaron-Becker, "Isolated broadband attosecond pulse generation with near- and mid-infrared driver pulses via time-gated phase matching," Opt. Express **25**, 11855–11866 (2017).
33. A. S. Johnson, D. R. Austin, D. A. Wood, C. Brahms, A. Gregory, K. B. Holzner, S. Jarosch, E. W. Larsen, S. Parker, C. S. Strüber, P. Ye, J. W. G. Tisch, and J. P. Marangos, "High-flux soft x-ray harmonic generation from ionization-shaped few-cycle laser pulses," Sci. Adv. **4**, eaar3761 (2018).
34. M. Ossiander, F. Siegrist, V. Shirvanyan, R. Pazourek, A. Sommer, T. Latka, A. Guggenmos, S. Nagele, J. Feist, J. Burgerdörfer, R. Kienberger, and M. Schultze, "Attosecond correlation dynamics," Nat. Phys. **13**, 280–285 (2016).
35. A. Baltuska, Th. Udem, M. Uiberacker, M. Hentschel, E. Goulielmakis, Ch. Gohle, R. Holzwarth, V. S. Yakovlev, A. Scrinzi, T. W. Hänsch, and F. Krausz, "Attosecond control of electronic processes by intense light fields," Nature **421**, 611–615 (2003).
36. E. Priori, G. Cerullo, M. Nisoli, S. Stagira, S. De Silvestri, P. Villoresi, L. Poletto, P. Ceccherini, C. Altucci, R. Bruzzese, and C. de Lisio, "Nonadiabatic three-dimensional model of high-order harmonic generation in the few-optical-cycle regime," Phys. Rev. A **61**, 063801 (2000).
37. V. Tosa, K. Kovács, B. Major, E. Balogh, and K. Varjú, "Propagation effects in highly ionised gas media," Quantum. Electron. **46**, 321–326 (2016).
38. K. Schmid and L. Veisz, "Supersonic gas jets for laser-plasma experiments," Rev. Sci. Instrum. **83**, 053304 (2012).
39. P. Saliéres, A. L'Huillier, and M. Lewenstein, "Coherence control of high-order harmonics," Phys. Rev. Lett. **74**, 3776–3779 (1995).
40. V. Tosa, J. S. Lee, H. T. Kim, and C. H. Nam, "Attosecond pulses generated by the lighthouse effect in Ar gas," Phys. Rev. A **91**, 051801 (2015).
41. K. Kovács, M. Negro, C. Vozzi, S. Stagira, and V. Tosa, "Attosecond lighthouse above 100 eV from high-harmonic generation of mid-infrared pulses," J. Opt. **19**, 104003 (2017).
42. A. Guggenmos, R. Rauhut, M. Hofstetter, S. Hertrich, B. Nickel, J. Schmidt, E. M. Gullikson, M. Seibald, W. Schnick, and U. Kleineberg, "Aperiodic CrSc multilayer mirrors for attosecond water window pulses," Opt. Express **21**, 21728–21740 (2013).
43. A. Guggenmos, M. Jobst, M. Ossiander, S. Radünz, J. Riemensberger, M. Schäffer, A. Akil, C. Jakubeit, P. Böhm, S. Noever, B. Nickel, R. Kienberger, and U. Kleineberg, "Chromium/scandium multilayer mirrors for isolated attosecond pulses at 145 eV," Opt. Lett. **40**, 2846–2849 (2015).
44. M. Schultze, B. Bergues, H. Schröder, F. Krausz, and K. L. Kompa, "Spatially resolved measurement of ionization yields in the focus of an intense laser pulse," New J. Phys. **13**, 033001 (2011).
45. F. Reiter, U. Graf, E. E. Serebryannikov, W. Schweinberger, M. Fiess, M. Schultze, A. M. Azzeer, R. Kienberger, F. Krausz, A. M. Zheltikov, and E. Goulielmakis, "Route to attosecond nonlinear spectroscopy," Phys. Rev. Lett. **105**, 243902 (2010).
46. S. Kühn, M. Dumergue, S. Kahaly, S. Mondal, M. Füle, T. Csizmadia, B. Farkas, B. Major, Z. Várallyay, E. Cormier, M. Kalashnikov, F. Calegari, M. Devetta, F. Frassetto, E. Månsson, L. Poletto, S. Stagira, C. Vozzi, M. Nisoli, P. Rudawski, S. Maclot, F. Campi, H. Wikmark, C. L. Arnold, C. M. Heyl, P. Johnsson, A. L'Huillier, R. Lopez-Martens, S. Haessler, M. Bocoum, F. Boehle, A. Vernier, G. Iaquaniello, E. Skantzakis, N. Papadakis, C. Kalpouzos, P. Tzallas, F. Lépine, D. Charalambidis, K. Varjú, K. Osvay, and G. Sansone, "The ELI-ALPS facility: the next generation of attosecond sources," J. Phys. B: At. Mol. Opt. Phys. **50**, 095004 (2017).
47. D. Rompotis, A. Baumann, O. Schepp, T. Maltezopoulos, M. Wieland, and M. Drescher, "Single-shot nonlinear spectroscopy in the vacuum-ultraviolet," Optica **4**, 871–878 (2017).